

Possible Realization of Kitaev Spin Liquids in van der Waals Heterostructures of $\alpha\text{-RuCl}_3$ and $\text{Cr}X_3$ ($X=\text{Cl}$ and I)

Lingzhi Zhang and Yukitoshi Motome

Department of Applied Physics, The University of Tokyo, Bunkyo, Tokyo 113-8656, Japan

(Dated: October 3, 2023)

Despite the presence of the exact solution and well-established recipe for its realization, the quest for the Kitaev spin liquid in real materials remains exceptionally challenging. Among many magnets, $\alpha\text{-RuCl}_3$ emerges as a prime candidate, albeit the hallmarks of the spin liquid manifest only within the specific region where the zigzag-type antiferromagnetic order is suppressed by an applied magnetic field. Here, we propose the possibility of the Kitaev spin liquid at zero field by making van der Waals heterostructures of $\alpha\text{-RuCl}_3$ and a ferromagnet $\text{Cr}X_3$ ($X=\text{Cl}$ and I). Using *ab initio* calculations, we find that in the case of $X=\text{Cl}$ the zigzag order is suppressed by the proximity effect of the ferromagnetic CrCl_3 layer, while the Kitaev interaction is still relevant in the $\alpha\text{-RuCl}_3$ layer. Notably, the induced Ru moment is close to the value observed in the spin liquid region of the bulk material, signifying the realization of the Kitaev spin liquid at zero field. In contrast, in the case of $X=\text{I}$, the system is on the verge of an insulator-metal transition by carrier doping through interlayer hybridization. Our results indicate that van der Waals heterostructures provide a new platform for studying not only magnetic but also electronic properties of the Kitaev magnets.

Introduction.— Since the successful exfoliation of graphene [1], van der Waals (vdW) materials have played a pivotal role in advancing two-dimensional physics [2–9]. The research forefront has been explosively expanded to diverse range of materials, such as elemental analogues of graphene [10–15], transition metal dichalcogenides [4, 16–19], and atomically thin magnets [9, 20–23]. Furthermore, the weak interlayer vdW force offers a wide platform for making heterostructures with emergent properties that cannot be found in individual materials [24–27]. Moiré superstructures in twisted multilayers have opened up yet another exciting avenue for manipulating electron correlation effects, exemplified by twisted bilayer graphene which realizes the Mott insulating state and superconductivity [28, 29].

Among the vdW materials, a transition metal trihalide $\alpha\text{-RuCl}_3$ has garnered significant attention due to its potential to realize the quantum spin liquid predicted in the Kitaev model [30]. The model is defined on a honeycomb lattice with bond-dependent Ising-type interaction between spin-1/2 moments, and the ground state is exactly obtained as a quantum spin liquid with fractional excitations, itinerant Majorana fermions and localized Z_2 fluxes, which can be utilized for topological quantum computation [31]. Since it was pointed out that spin-orbit entangled moments can yield the Kitaev-type interaction [32], many materials with both electron correlation and spin-orbit coupling, called the spin-orbit coupled Mott insulators, have been investigated as potential candidates for the Kitaev spin liquid (KSL) [33–37]. Notably, $\alpha\text{-RuCl}_3$ is a primary candidate, as it exhibits hallmarks of the KSL, as identified by several experimental techniques, such as Raman scattering [38–40], inelastic neutron scattering [41–43], and half-quantization of the thermal Hall conductivity [44, 45].

Despite the promising hallmarks, the problem is that the KSL appears to manifest only under the magnetic field at low temperatures, which hampers in-depth ex-

perimental investigations. This issue stems from the fact that, in the absence of the magnetic field, the system exhibits a zigzag-type magnetic order due to parasitic magnetic interactions beyond the Kitaev model [46–48]. The spin liquid nature is observed only in a regime where the zigzag order is destroyed by an applied magnetic field of ~ 8 T. Extensive efforts have been made to suppress the zigzag order by mitigating the parasitic interactions. For instance, theoretical research has suggested that lattice expansion can suppress the non-Kitaev interactions [49–51], stimulating the fabrication of thin films and their heterostructures [52–57]. Nonetheless, establishing a method to realize the KSL at zero field remains a challenging issue, despite its crucial significance for experimental accessibility.

In this Letter, we propose a way to achieve the KSL at zero magnetic field by employing vdW heterostructures. The key idea is to suppress the zigzag order through the proximity effect of vdW magnets, $\text{Cr}X_3$ with $X=\text{Cl}$ and I . CrCl_3 and CrI_3 were recently shown, respectively, to exhibit in-plane and out-of plane ferromagnetism in their monolayer form [22, 58]. Based on *ab initio* calculations, we show that an internal magnetic field and interlayer hybridization from the $\text{Cr}X_3$ layer have a profound impact on the magnetic and electronic properties of the $\alpha\text{-RuCl}_3$ layer, offering a promising route to a possible KSL at zero field.

Methods.— We consider two heterostructures: One consists of an $\alpha\text{-RuCl}_3$ layer and a CrCl_3 layer ($\alpha\text{-RuCl}_3/\text{CrCl}_3$) [Fig. 1(a)], and the other consists of an $\alpha\text{-RuCl}_3$ layer and a CrI_3 layer ($\alpha\text{-RuCl}_3/\text{CrI}_3$) [Fig. 1(b)]. For both cases, the lattice structure of each layer is taken from the bulk materials with $C2/m$ symmetry [47, 59, 60]. For $\alpha\text{-RuCl}_3/\text{CrCl}_3$, because of the small lattice mismatch between $\alpha\text{-RuCl}_3$ (5.97 Å) and CrCl_3 (5.96 Å), we prepare the heterostructure supercell by stacking each unit cell as is, which contains 16 atoms in total. Meanwhile, for $\alpha\text{-RuCl}_3/\text{CrI}_3$, due to the large lattice mis-

TABLE I. Energy per Ru atom and magnetic moments at Ru and Cr atoms for different magnetic states in $\alpha\text{-RuCl}_3/\text{CrCl}_3$ obtained by the *ab initio* calculations: “in” and “out” means that the magnetic moment is along the in-plane and out-of-plane direction, respectively, and “FM”, “Néel”, and “zigzag” denote ferromagnetic, Néel, and zigzag orders, respectively. The prime indicates that the Cr moments are antiparallel to the Ru ones (otherwise, they are parallel). The energy is measured from the most stable state where the in-plane FM order in each layer is coupled antiferromagnetically.

magnetic state		energy/Ru (meV)	moment (μ_B)	
Ru	Cr		Ru	Cr
in-FM	in-FM'	0.000	0.703	3.28
in-FM	out-FM	0.365	0.703	3.28
in-FM	in-FM	0.775	0.704	3.28
in-zigzag	in-FM	6.32	0.579	3.28
in-Néel	in-FM	16.2	0.293	3.28
out-FM	out-FM	105	0.834	3.28
out-FM	out-FM'	104	0.832	3.28

match between $\alpha\text{-RuCl}_3$ (5.97 Å) and CrI_3 (6.86 Å), we prepare the heterostructure supercell by 2×2 $\alpha\text{-RuCl}_3$ and $\sqrt{3} \times \sqrt{3}$ CrI_3 , containing 56 atoms. We optimize the lattice structures via the nonrelativistic *ab initio* calculations described below, by relaxing the atomic positions with fixing the in-plane lattice constants of $\alpha\text{-RuCl}_3$ at the bulk value. After the relaxation, the interlayer distance is optimized to 3.01 Å for $\alpha\text{-RuCl}_3/\text{CrCl}_3$ and 3.22 Å for $\alpha\text{-RuCl}_3/\text{CrCl}_3$.

We perform the *ab initio* calculations based on the density functional theory (DFT) using the OpenMX code [61, 62]. We use the Perdew-Burke-Ernzerhof generalized gradient approximation (GGA-PBE) functional [63] including U corrections for Ru d orbitals and Cr d orbitals, as implemented in the GGA+ U method [64]; we take $U = 1.5$ eV for Ru and $U = 2.0$ eV for Cr [65, 66]. The kinetic energy cutoffs are set to be 1500 Ry. VdW corrections are also included through the DFT-D2 scheme of Grimme [67]. In the self-consistent calculation of the electron density, we take $16 \times 16 \times 1$ k -point mesh for $\alpha\text{-RuCl}_3/\text{CrCl}_3$ and $10 \times 10 \times 1$ k -point mesh for $\alpha\text{-RuCl}_3/\text{CrI}_3$. We construct maximally-localized Wannier functions [68, 69] for the electronic band structures obtained by the DFT calculation and use them to compute the partial density of states (PDOS) and effective exchange constants. For the latter, we perform the second-order perturbation for the multiorbital Hubbard model for t_{2g} orbitals of Ru atoms, following the previous studies [49, 70, 71]. In this model, we set the effective onsite Coulomb interaction \tilde{U} , the Hund’s rule coupling J_H , and the spin-orbit coupling coefficient λ to 3.0 eV, 0.6 eV, and 0.15 eV, respectively [49].

Results.— For the optimized heterostructures, we investigate the energies of different magnetically ordered states by utilizing the constraint DFT calculation on the direction of magnetic moments. The results for $\alpha\text{-RuCl}_3/\text{CrCl}_3$ are listed in Table I. We obtain seven stable

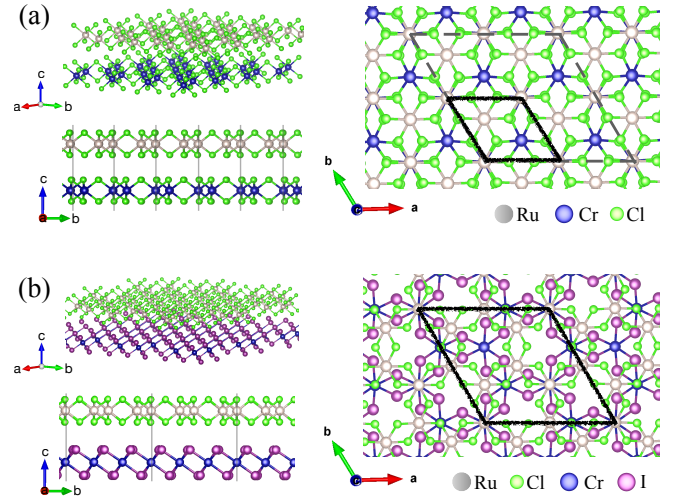


FIG. 1. Structures of the heterostructures of $\alpha\text{-RuCl}_3$ and CrX_3 ($X=\text{Cl}$ and I). (a) A bird’s-eye view (upper left), side view (lower left), and top view (right) of $\alpha\text{-RuCl}_3/\text{CrCl}_3$. (b) Corresponding pictures for $\alpha\text{-RuCl}_3/\text{CrI}_3$. The gray, blue, green, and purple spheres represent Ru, Cr, Cl, and I atoms, respectively. The black rhombus denotes the unit cell, while the gray dashed rhombus in (a) is a 2×2 supercell used in the *ab initio* calculations.

TABLE II. Similar table for $\alpha\text{-RuCl}_3/\text{CrI}_3$: “cant” means a spin canting, and the other notations are common to Table I.

magnetic state		energy/Ru (meV)	moment (μ_B)	
Ru	Cr		Ru	Cr
in-FM	cant-FM	0.000	0.675	3.73
in-FM	out-FM	0.359	0.673	3.73
in-FM	in-FM'	0.443	0.678	3.73
in-FM	in-FM	3.14	0.673	3.73
in-zigzag	out-FM	8.42	0.571	3.73

magnetic states, and among them the most stable is the intralayer-ferromagnetic (FM) and interlayer antiferromagnetic (AFM) state with in-plane magnetic moments of $0.703 \mu_B$ for Ru and $3.28 \mu_B$ for Cr. Notably, the intralayer FM states with different Cr moment directions are obtained at slightly higher energies: the state with out-of-plane Cr moments at 0.365 meV and in-plane Cr moments parallel to the Ru ones at 0.775 meV. This suggests that the Cr layer has in-plane ferromagnetism similarly to the monolayer [58], but the magnetic anisotropy is small and the energy scale of the interlayer magnetic coupling in this heterostructure is the order of 0.1 meV (see Supplementary Material [72]). The next higher-energy state at 6.32 meV exhibits a zigzag order in the Ru layer. While the stable magnetic state for the $\alpha\text{-RuCl}_3$ monolayer is still controversial [73–76], our result indicates that the heterostructure with CrCl_3 favors the FM state in the $\alpha\text{-RuCl}_3$ layer, rather than the zigzag order that is stable in the bulk. We will discuss this interesting point later. The other states have much higher energies;

in particular, the states with out-of-plane Ru moments are more than 100 meV higher, indicating that the strong in-plane magnetic anisotropy in the bulk α -RuCl₃ is retained even in the heterostructure [60, 77–79].

The results for α -RuCl₃/CrI₃ are summarized in Table II. In this case also, we find that the most stable state exhibits FM ordering in each layer, whereas the Cr moments are canted about 30 degrees from the out-of-plane in the opposite direction to the Ru moments. This is understood from the fact that the monolayer CrI₃ is an out-of-plane ferromagnet [22]. Nonetheless, similarly to the case of α -RuCl₃/CrCl₃, the energy differences from the states with other Cr moment directions are rather small, while the zigzag order in the Ru layer leads to relatively higher energy (see Supplementary Material [72]).

For the most stable states obtained above, we calculate the band structures and the PDOS. For α -RuCl₃/CrCl₃ [Fig. 2(a)], we find that the low-energy state near the Fermi level is dominated by the spin-orbital coupled bands characterized by the pseudospin $j_{\text{eff}} = 1/2$ and 3/2 hybridized with 3p orbitals of Cl atoms in the α -RuCl₃ layer. The system is an insulator with the energy gap of ~ 0.6 eV opening in the pseudospin bands. The situation is very similar to the bulk α -RuCl₃, where the spin-orbit coupling and electron correlation work cooperatively to realize a spin-orbit coupled Mott insulating state [30, 80, 81]. The contribution from CrCl₃ appears well below the Fermi level, and does not disturb the low-energy pseudospin bands of Ru atoms.

Meanwhile, in α -RuCl₃/CrI₃, the spin-orbital coupled features are preserved in the pseudospin bands, but the band gap is largely reduced [Fig. 2(b)]. This is due to considerable contributions from the 5p orbitals of I atoms, in contrast to the Cl 3p orbitals in the case of α -RuCl₃/CrCl₃. The enlarged plot near the Fermi level is shown in Fig. 3. We find that there still remains a small gap of ~ 0.02 eV, but the system is on the verge of an insulator-metal transition, and the $j_{\text{eff}} = 1/2$ band is slightly doped below the small gap through the hybridization with the 5p bands.

To understand the differences in the band structures between the two heterostructures, we compute real-space distributions of electron charges. Figure 4 displays the charge-density difference between the heterostructure and two independent monolayers, $\delta\rho(\alpha\text{-RuCl}_3/\text{Cr}X_3) = \rho(\alpha\text{-RuCl}_3/\text{Cr}X_3) - \rho(\alpha\text{-RuCl}_3) - \rho(\text{Cr}X_3)$, with the iso-surface of 5×10^{-4} e/ \AA^3 . In α -RuCl₃/CrCl₃ [Fig. 4(a)], while the charge distribution in the α -RuCl₃ layer is modulated, the original symmetry is overall retained, with little changes in the interlayer region. This is consistent with the robust pseudospin bands in Fig. 2(a). In contrast, in α -RuCl₃/CrI₃ [Fig. 4(b)], the charge distributions near the Cl and I atoms at the interface are largely modulated and extended to the interlayer region. We observe that approximately 0.021e per unit cell of α -RuCl₃ is transferred from the CrI₃ layer. These are consistent with the large modulation of the band structure with carrier doping through the hybridization with 5p orbitals of

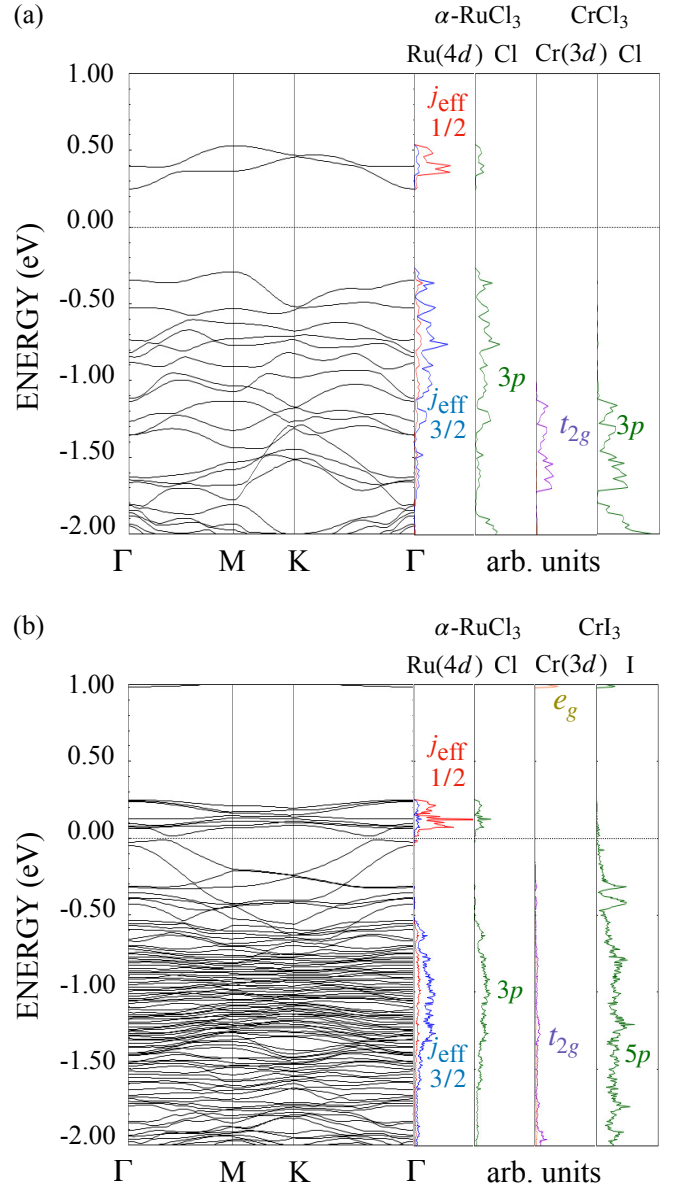


FIG. 2. Band structure and PDOS in the most stable magnetic states: (a) the Ru in-FM and Cr in FM' state for α -RuCl₃/CrCl₃ and (b) the Ru In-FM and Cr cant-FM state for α -RuCl₃/CrI₃. The Fermi level is set at zero energy.

I atoms found in Figs. 2(b) and 3.

Given that the spin-orbit coupled Mott insulating nature is preserved in the α -RuCl₃ layer of α -RuCl₃/CrCl₃, we estimate effective exchange constants between the $j_{\text{eff}} = 1/2$ pseudospins, using the procedure described above. The general expression of the effective pseudospin Hamiltonian for one of three types of bonds on the honeycomb lattice is given by

$$\mathcal{H}_{ij}^z = \mathbf{S}_i^T \begin{bmatrix} J & D + \Gamma & -D' + \Gamma' \\ -D + \Gamma & J & D' + \Gamma' \\ D' + \Gamma' & -D' + \Gamma' & J + K \end{bmatrix} \mathbf{S}_j, \quad (1)$$

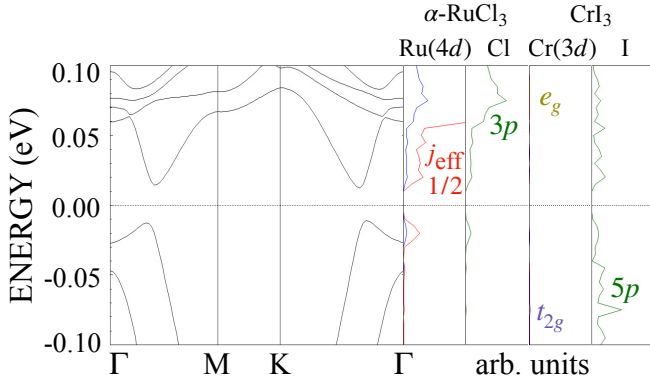


FIG. 3. Enlarged band structure and PDOS near the Fermi level for $\alpha\text{-RuCl}_3/\text{CrI}_3$ in Fig. 2(b).

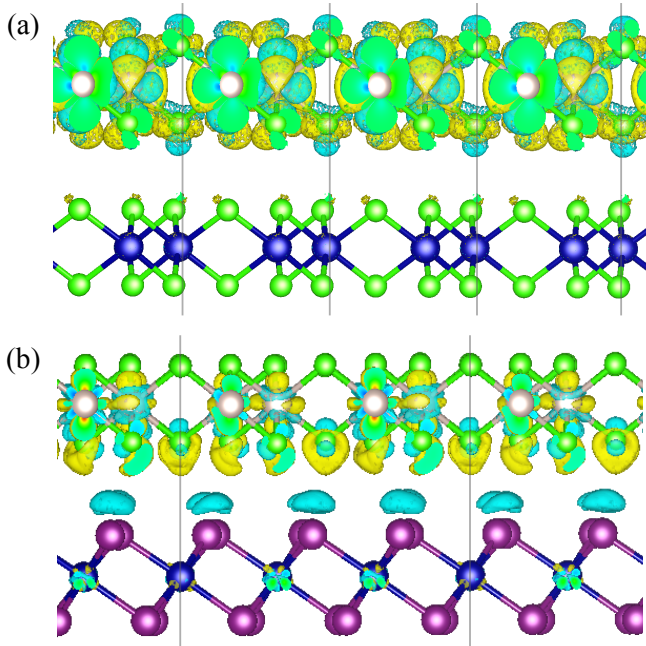


FIG. 4. Charge-density difference $\delta\rho$ plotted with charge isosurface $5 \times 10^{-4} \text{ e}/\text{\AA}^3$ of (a) $\alpha\text{-RuCl}_3/\text{CrCl}_3$ and (b) $\alpha\text{-RuCl}_3/\text{CrI}_3$. Both are viewed from the a axis of the $\alpha\text{-RuCl}_3$ layer. The yellow (cyan) color represents regions with charge accumulation (deficiency) compared to independent monolayers. The gray, blue, green, and purple spheres represent Ru, Cr, Cl, and I atoms, respectively.

where J and K denote the Heisenberg and Kitaev interactions, respectively, Γ and Γ' denote the symmetric off-diagonal interactions, and D and D' denote the anti-symmetric off-diagonal Dzyaloshinskii-Moriya (DM) interactions. The estimates of the exchange constants are listed in Table III, in comparison with the results for the monolayer (obtained in the present study) and bulk of $\alpha\text{-RuCl}_3$ [49]. Compared to the bulk, we find that in $\alpha\text{-RuCl}_3/\text{CrCl}_3$ the Heisenberg J is largely suppressed and the Kitaev K is enhanced, leading to the signifi-

TABLE III. Effective exchange constants between the $j_{\text{eff}} = 1/2$ pseudospins at the Ru sites for $\alpha\text{-RuCl}_3/\text{CrCl}_3$, in comparison with those for the monolayer and bulk of $\alpha\text{-RuCl}_3$. The energy unit is meV.

	J	K	Γ	Γ'	D	D'	K/J
$\alpha\text{-RuCl}_3/\text{CrCl}_3$	-0.9	-5.9	6.6	-1.6	-0.1	-0.1	6.6
$\alpha\text{-RuCl}_3$ (monolayer)	-1.0	-6.6	7.1	-2.0	0.0	0.0	6.6
$\alpha\text{-RuCl}_3$ (bulk) [49]	-2.2	-5.0	8.0	-1.0	0.0	0.0	2.3

cant increase of the ratio K/J . Meanwhile, the values are similar to those for the monolayer, despite the charge modulation in Fig. 4(a). This means that the suppression of the zigzag order is ascribed to the synergetic effect between the modulation of the exchange constants from the bulk to monolayer and the internal magnetic field from the ferromagnetic CrCl_3 layer in the heterostructure.

Discussion.— In $\alpha\text{-RuCl}_3/\text{CrCl}_3$, the zigzag order in $\alpha\text{-RuCl}_3$ is suppressed by the proximity effect of CrCl_3 , and replaced by the FM state with Ru moment of $0.703 \mu_B$. Notably, this value is close to that in the spin liquid region in the bulk system where the zigzag order is destroyed by an in-plane magnetic field [47] and the half-quantization of the thermal Hall conductivity was observed [44, 45]. This, in conjunction with the dominant Kitaev interaction in Table III, suggests the possibility of KSL at zero field under the proximity effect in the vdW heterostructure.

In $\alpha\text{-RuCl}_3/\text{CrCl}_3$, while the spin-orbit Mott insulating nature is preserved in the Ru pseudospin bands, the band gap is almost closing and the self-doping occurs via the interlayer hybridization. A similar situation was found in the heterostructure of $\alpha\text{-RuCl}_3$ and graphene [55, 56, 82, 83], where the system becomes metallic. Thus, the vdW heterostructures offer a playground for the insulator-metal transition in the spin-orbital coupled systems by carrier doping, which is expected to bring about exotic quantum phenomena such as topological superconductivity [84–87]. This is complementary to bandwidth control, which has recently been studied for the bulk materials RuX_3 ($X=\text{Cl}, \text{Br}$, and I) [88–91].

Summary.— We have investigated the vdW heterostructures composed of the Kitaev candidate $\alpha\text{-RuCl}_3$ and the ferromagnet CrX_3 ($X=\text{Cl}$ and I) based on the *ab initio* calculations. For $\alpha\text{-RuCl}_3/\text{CrCl}_3$, we found that the zigzag order in $\alpha\text{-RuCl}_3$ is replaced by an in-plane FM state with the Ru moment close to that in the region where the hallmarks of KSL were observed in the bulk material. We also showed that the Kitaev interaction between the Ru pseudospins is enhanced. These suggest that the proximity of CrCl_3 realizes the KSL in the $\alpha\text{-RuCl}_3$ layer even in the absence of magnetic field. In $\alpha\text{-RuCl}_3/\text{CrI}_3$, we found that the system is on the verge of insulator-metal transition due to charge transfer from CrI_3 via the strong interlayer hybridization, while the spin-orbit coupled Mott insulating nature is preserved.

Our findings unveil that the vdW heterostructures enable us to access the KSL physics at zero field, which is hard to achieve in the bulk system. The diverse range of materials and their flexible stacking control in vdW systems open up possibilities for tailoring the electronic and magnetic properties in the Kitaev magnets.

We thank S.-H. Jang, Y. Kato, S. Okumura, and Y..

F. Zhao for fruitful discussions. This research was supported by the JSPS KAKENHI (Nos. JP19H05825 and JP20H00122) and JST CREST (No. JP-MJCR18T2). Parts of the numerical calculations were performed using the facilities of the Supercomputer Center, the Institute for Solid State Physics, the University of Tokyo.

-
- [1] K. S. Novoselov, A. K. Geim, S. V. Morozov, D. Jiang, Y. Zhang, S. V. Dubonos, I. V. Grigorieva, and A. A. Firsov, Electric Field Effect in Atomically Thin Carbon Films, *Science* **306**, 666 (2004).
- [2] A. K. Geim and K. S. Novoselov, The rise of graphene, *Nat. Mater.* **6**, 183 (2007).
- [3] A. K. Geim, Graphene: Status and Prospects, *Science* **324**, 1530 (2009).
- [4] Q. H. Wang, K. Kalantar-Zadeh, A. Kis, J. N. Coleman, and M. S. Strano, Electronics and optoelectronics of two-dimensional transition metal dichalcogenides, *Nat. Nanotechnol.* **7**, 699 (2012).
- [5] M. Xu, T. Liang, M. Shi, and H. Chen, Graphene-Like Two-Dimensional Materials, *Chem. Rev.* **113**, 3766 (2013).
- [6] K. S. Novoselov, A. Mishchenko, A. Carvalho, and A. H. C. Neto, 2D materials and van der Waals heterostructures, *Science* **353**, aac9439 (2016).
- [7] J.-G. Park, Opportunities and challenges of 2D magnetic van der Waals materials: magnetic graphene?, *J. Phys.: Condens. Matter* **28**, 301001 (2016).
- [8] S. Manzeli, D. Ovchinnikov, D. Pasquier, O. V. Yazyev, and A. Kis, 2D transition metal dichalcogenides, *Nat. Rev. Mater.* **2**, 17033 (2017).
- [9] K. S. Burch, D. Mandrus, and J.-G. Park, Magnetism in two-dimensional van der Waals materials, *Nature* **563**, 47 (2018).
- [10] K. Takeda and K. Shiraishi, Theoretical possibility of stage corrugation in Si and Ge analogs of graphite, *Phys. Rev. B* **50**, 14916 (1994).
- [11] S. Cahangirov, M. Topsakal, E. Aktürk, H. Şahin, and S. Ciraci, Two- and One-Dimensional Honeycomb Structures of Silicon and Germanium, *Phys. Rev. Lett.* **102**, 236804 (2009).
- [12] P. Vogt, P. De Padova, C. Quaresima, J. Avila, E. Frantzeskakis, M. C. Asensio, A. Resta, B. Ealet, and G. Le Lay, Silicene: Compelling Experimental Evidence for Graphenelike Two-Dimensional Silicon, *Phys. Rev. Lett.* **108**, 155501 (2012).
- [13] A. Fleurence, R. Friedlein, T. Ozaki, H. Kawai, Y. Wang, and Y. Yamada-Takamura, Experimental Evidence for Epitaxial Silicene on Diboride Thin Films, *Phys. Rev. Lett.* **108**, 245501 (2012).
- [14] M. E. Dávila, L. Xian, S. Cahangirov, A. Rubio, and G. L. Lay, Germanene: a novel two-dimensional germanium allotrope akin to graphene and silicene, *New J. Phys.* **16**, 095002 (2014).
- [15] F.-f. Zhu, W.-j. Chen, Y. Xu, C.-l. Gao, D.-d. Guan, C.-h. Liu, D. Qian, S.-C. Zhang, and J.-f. Jia, Epitaxial growth of two-dimensional stanene, *Nat. Mater.* **14**, 1020 (2015).
- [16] A. Splendiani, L. Sun, Y. Zhang, T. Li, J. Kim, C.-Y. Chim, G. Galli, and F. Wang, Emerging photoluminescence in monolayer MoS₂, *Nano Lett.* **10**, 1271 (2010).
- [17] K. F. Mak, C. Lee, J. Hone, J. Shan, and T. F. Heinz, Atomically Thin MoS₂: A New Direct-Gap Semiconductor, *Phys. Rev. Lett.* **105**, 136805 (2010).
- [18] K. F. Mak, K. L. McGill, J. Park, and P. L. McEuen, The valley Hall effect in MoS₂ transistors, *Science* **344**, 1489 (2014).
- [19] W.-Y. Tong, S.-J. Gong, X. Wan, and C.-G. Duan, Concepts of ferrovalley material and anomalous valley Hall effect, *Nat. Commun.* **7**, 13612 (2016).
- [20] J.-U. Lee, S. Lee, J. H. Ryoo, S. Kang, T. Y. Kim, P. Kim, C.-H. Park, J.-G. Park, and H. Cheong, Ising-type magnetic ordering in atomically thin FePS₃, *Nano Lett.* **16**, 7433 (2016).
- [21] C. Gong, L. Li, Z. Li, H. Ji, A. Stern, Y. Xia, T. Cao, W. Bao, C. Wang, Y. Wang, Z. Q. Qiu, R. J. Cava, S. G. Louie, J. Xia, and X. Zhang, Discovery of intrinsic ferromagnetism in two-dimensional van der Waals crystals, *Nature* **546**, 265 (2017).
- [22] B. Huang, G. Clark, E. Navarro-Moratalla, D. R. Klein, R. Cheng, K. L. Seyler, D. Zhong, E. Schmidgall, M. A. McGuire, D. H. Cobden, W. Yao, D. Xiao, P. Jarillo-Herrero, and X. Xu, Layer-dependent ferromagnetism in a van der Waals crystal down to the monolayer limit, *Nature* **546**, 270 (2017).
- [23] C. Gong and X. Zhang, Two-dimensional magnetic crystals and emergent heterostructure devices, *Science* **363**, eaav4450 (2019).
- [24] A. K. Geim and I. V. Grigorieva, Van der Waals heterostructures, *Nature* **499**, 419 (2013).
- [25] Y. Liu, N. O. Weiss, X. Duan, H.-C. Cheng, Y. Huang, and X. Duan, Van der Waals heterostructures and devices, *Nat. Rev. Mater.* **1**, 16042 (2016).
- [26] M. Gibertini, M. Koperski, A. F. Morpurgo, and K. S. Novoselov, Magnetic 2D materials and heterostructures, *Nat. Nanotechnol.* **14**, 408 (2019).
- [27] J. Li, X. Yang, Y. Liu, B. Huang, R. Wu, Z. Zhang, B. Zhao, H. Ma, W. Dang, Z. Wei, K. Wang, Z. Lin, X. Yan, M. Sun, B. Li, X. Pan, J. Luo, G. Zhang, Y. Liu, Y. Huang, X. Duan, and X. Duan, General synthesis of two-dimensional van der Waals heterostructure arrays, *Nature* **579**, 368 (2020).
- [28] Y. Cao, V. Fatemi, S. Fang, K. Watanabe, T. Taniguchi, E. Kaxiras, and P. Jarillo-Herrero, Unconventional superconductivity in magic-angle graphene superlattices, *Nature* **556**, 43 (2018).
- [29] E. Y. Andrei and A. H. MacDonald, Graphene bilayers with a twist, *Nat. Mater.* **19**, 1265 (2020).
- [30] K. W. Plumb, J. P. Clancy, L. J. Sandilands, V. V. Shankar, Y. F. Hu, K. S. Burch, H.-Y. Kee, and Y.-J. Kim, α -RuCl₃: A spin-orbit assisted Mott insulator on a

- honeycomb lattice, Phys. Rev. B **90**, 041112 (2014).
- [31] A. Kitaev, Anyons in an exactly solved model and beyond, Ann. Phys. (Amsterdam) **321**, 2 (2006).
- [32] G. Jackeli and G. Khaliullin, Mott Insulators in the Strong Spin-Orbit Coupling Limit: From Heisenberg to a Quantum Compass and Kitaev Models, Phys. Rev. Lett. **102**, 017205 (2009).
- [33] S. M. Winter, A. A. Tsirlin, M. Daghofer, J. van den Brink, Y. Singh, P. Gegenwart, and R. Valentí, Models and materials for generalized Kitaev magnetism, J. Phys.: Condens. Matter **29**, 493002 (2017).
- [34] H. Takagi, T. Takayama, G. Jackeli, G. Khaliullin, and S. E. Nagler, Concept and realization of Kitaev quantum spin liquids, Nat. Rev. Phys. **1**, 264 (2019).
- [35] Y. Motome and J. Nasu, Hunting Majorana Fermions in Kitaev Magnets, J. Phys. Soc. Japan **89**, 012002 (2020).
- [36] Y. Motome, R. Sano, S. Jang, Y. Sugita, and Y. Kato, Materials design of Kitaev spin liquids beyond the Jackeli-Khaliullin mechanism, J. Phys.: Condens. Matter **32**, 404001 (2020).
- [37] S. Trebst and C. Hickey, Kitaev materials, Phys. Rep. **950**, 1 (2022).
- [38] L. J. Sandilands, Y. Tian, K. W. Plumb, Y.-J. Kim, and K. S. Burch, Scattering Continuum and Possible Fractionalized Excitations in α -RuCl₃, Phys. Rev. Lett. **114**, 147201 (2015).
- [39] J. Nasu, J. Knolle, D. L. Kovrizhin, Y. Motome, and R. Moessner, Fermionic response from fractionalization in an insulating two-dimensional magnet, Nat. Phys. **12**, 912 (2016).
- [40] Y. Wang, G. B. Osterhoudt, Y. Tian, P. Lampen-Kelley, A. Banerjee, T. Goldstein, J. Yan, J. Knolle, H. Ji, R. J. Cava, J. Nasu, Y. Motome, S. E. Nagler, D. Mandrus, and K. S. Burch, The range of non-Kitaev terms and fractional particles in α -RuCl₃, npj Quantum Materials **5**, 14 (2020).
- [41] A. Banerjee, C. Bridges, J.-Q. Yan, A. Aczel, L. Li, M. Stone, G. Granroth, M. Lumsden, Y. Yiu, J. Knolle, S. Bhattacharjee, D. L. Kovrizhin, R. Moessner, D. A. Tennant, D. G. Mandrus, and S. E. Nagler, Proximate Kitaev quantum spin liquid behaviour in a honeycomb magnet, Nat. Mater. **15**, 733 (2016).
- [42] S.-H. Do, S.-Y. Park, J. Yoshitake, J. Nasu, Y. Motome, Y. S. Kwon, D. Adroja, D. Voneshen, K. Kim, T.-H. Jang, J.-H. Park, K.-Y. Choi, and S. Ji, Majorana fermions in the Kitaev quantum spin system α -RuCl₃, Nat. Phys. **13**, 1079 (2017).
- [43] A. Banerjee, P. Lampen-Kelley, J. Knolle, C. Balz, A. A. Aczel, B. Winn, Y. Liu, D. Pajerowski, J. Yan, C. A. Bridges, A. T. Savici, B. C. Chakoumakos, M. D. Lumsden, D. A. Tennant, R. Moessner, D. G. Mandrus, and S. E. Nagler, Excitations in the field-induced quantum spin liquid state of α -RuCl₃, npj Quantum Materials **3**, 8 (2018).
- [44] Y. Kasahara, T. Ohnishi, Y. Mizukami, O. Tanaka, S. Ma, K. Sugii, N. Kurita, H. Tanaka, J. Nasu, Y. Motome, T. Shibauchi, and Y. Matsuda, Majorana quantization and half-integer thermal quantum Hall effect in a Kitaev spin liquid, Nature **559**, 227 (2018).
- [45] T. Yokoi, S. Ma, Y. Kasahara, S. Kasahara, T. Shibauchi, N. Kurita, H. Tanaka, J. Nasu, Y. Motome, C. Hickey, S. Trebst, and Y. Matsuda, Half-integer quantized anomalous thermal Hall effect in the Kitaev material candidate α -RuCl₃, Science **373**, 568 (2021).
- [46] J. A. Sears, M. Songvilay, K. W. Plumb, J. P. Clancy, Y. Qiu, Y. Zhao, D. Parshall, and Y.-J. Kim, Magnetic order in α -RuCl₃: A honeycomb-lattice quantum magnet with strong spin-orbit coupling, Phys. Rev. B **91**, 144420 (2015).
- [47] R. D. Johnson, S. C. Williams, A. A. Haghishirad, J. Singleton, V. Zapf, P. Manuel, I. I. Mazin, Y. Li, H. O. Jeschke, R. Valentí, and R. Coldea, Monoclinic crystal structure of α -RuCl₃ and the zigzag antiferromagnetic ground state, Phys. Rev. B **92**, 235119 (2015).
- [48] H. B. Cao, A. Banerjee, J.-Q. Yan, C. A. Bridges, M. D. Lumsden, D. G. Mandrus, D. A. Tennant, B. C. Chakoumakos, and S. E. Nagler, Low-temperature crystal and magnetic structure of α -RuCl₃, Phys. Rev. B **93**, 134423 (2016).
- [49] S. M. Winter, Y. Li, H. O. Jeschke, and R. Valentí, Challenges in design of Kitaev materials: Magnetic interactions from competing energy scales, Phys. Rev. B **93**, 214431 (2016).
- [50] R. Yadav, S. Rachel, L. Hozoi, J. van den Brink, and G. Jackeli, Strain- and pressure-tuned magnetic interactions in honeycomb kитаev materials, Phys. Rev. B **98**, 121107 (2018).
- [51] D. A. S. Kaib, S. Biswas, K. Riedl, S. M. Winter, and R. Valentí, Magnetoelastic coupling and effects of uniaxial strain in α -RuCl₃ from first principles, Phys. Rev. B **103**, L140402 (2021).
- [52] M. Ziatdinov, A. Banerjee, A. Maksov, T. Berlijn, W. Zhou, H. Cao, J.-Q. Yan, C. A. Bridges, D. Mandrus, S. E. Nagler, A. P. Baddorf, and S. V. Kalinin, Atomic-scale observation of structural and electronic orders in the layered compound α -RuCl₃, Nat. Commun. **7**, 13774 (2016).
- [53] D. Weber, L. M. Schoop, V. Duppel, J. M. Lippmann, J. Nuss, and B. V. Lotsch, Magnetic Properties of Restacked 2D Spin 1/2 honeycomb RuCl₃ Nanosheets, Nano Lett. **16**, 3578 (2016).
- [54] B. Zhou, Y. Wang, G. B. Osterhoudt, P. Lampen-Kelley, D. Mandrus, R. He, K. S. Burch, and E. A. Henriksen, Possible structural transformation and enhanced magnetic fluctuations in exfoliated α -RuCl₃, J. Phys. Chem. Solids **128**, 291 (2019).
- [55] S. Mashhadi, Y. Kim, J. Kim, D. Weber, T. Taniguchi, K. Watanabe, N. Park, B. Lotsch, J. H. Smet, M. Burghard, and K. Kern, Spin-Split Band Hybridization in Graphene Proximity-Induced with α -RuCl₃ Nanosheets, Nano Lett. **19**, 4659 (2019).
- [56] B. Zhou, J. Balgley, P. Lampen-Kelley, J.-Q. Yan, D. G. Mandrus, and E. A. Henriksen, Evidence for charge transfer and proximate magnetism in graphene- α -RuCl₃ heterostructures, Phys. Rev. B **100**, 165426 (2019).
- [57] Z. Wang, L. Liu, H. Zheng, M. Zhao, K. Yang, C. Wang, F. Yang, H. Wu, and C. Gao, Direct observation of the Mottness and p-d orbital hybridization in the epitaxial monolayer α -RuCl₃, Nanoscale **14**, 11745 (2022).
- [58] A. Bedoya-Pinto, J.-R. Ji, A. K. Pandeya, P. Gargiani, M. Valvidares, P. Sessi, J. M. Taylor, F. Radu, K. Chang, and S. S. P. Parkin, Intrinsic 2D-XY ferromagnetism in a van der Waals monolayer, Science **374**, 616 (2021).
- [59] B. Morosin and A. Narath, X-Ray Diffraction and Nuclear Quadrupole Resonance Studies of Chromium Trichloride, J. Chem. Phys. **40**, 1958 (2004).
- [60] M. A. McGuire, H. Dixit, V. R. Cooper, and B. C. Sales, Coupling of Crystal Structure and Magnetism in the Lay-

- ered, Ferromagnetic Insulator CrI_3 , *Chem. Mater.* **27**, 612 (2015).
- [61] T. Ozaki, Variationally optimized atomic orbitals for large-scale electronic structures, *Phys. Rev. B* **67**, 155108 (2003).
- [62] T. Ozaki and H. Kino, Numerical atomic basis orbitals from H to Kr, *Phys. Rev. B* **69**, 195113 (2004).
- [63] J. P. Perdew, K. Burke, and M. Ernzerhof, Generalized Gradient Approximation Made Simple, *Phys. Rev. Lett.* **77**, 3865 (1996).
- [64] S. L. Dudarev, G. A. Botton, S. Y. Savrasov, C. J. Humphreys, and A. P. Sutton, Electron-energy-loss spectra and the structural stability of nickel oxide: An LSDA+U study, *Phys. Rev. B* **57**, 1505 (1998).
- [65] T. Biesner, S. Biswas, W. Li, Y. Saito, A. Pustogow, M. Altmeyer, A. U. B. Wolter, B. Büchner, M. Roslova, T. Doert, S. M. Winter, R. Valentí, and M. Dressel, Detuning the honeycomb of $\alpha\text{-RuCl}_3$: Pressure-dependent optical studies reveal broken symmetry, *Phys. Rev. B* **97**, 220401 (2018).
- [66] J. L. Lado and J. Fernández-Rossier, On the origin of magnetic anisotropy in two dimensional CrI_3 , *2D Mater.* **4**, 035002 (2017).
- [67] S. Grimme, Semiempirical GGA-type density functional constructed with a long-range dispersion correction, *J Comput Chem* **27**, 1787 (2006).
- [68] N. Marzari and D. Vanderbilt, Maximally localized generalized Wannier functions for composite energy bands, *Phys. Rev. B* **56**, 12847 (1997).
- [69] I. Souza, N. Marzari, and D. Vanderbilt, Maximally localized Wannier functions for entangled energy bands, *Phys. Rev. B* **65**, 035109 (2001).
- [70] Y. Yamaji, Y. Nomura, M. Kurita, R. Arita, and M. Imada, First-Principles Study of the Honeycomb-Lattice Iridates Na_2IrO_3 in the Presence of Strong Spin-Orbit Interaction and Electron Correlations, *Phys. Rev. Lett.* **113**, 107201 (2014).
- [71] Y. Sugita, Y. Kato, and Y. Motome, Antiferromagnetic Kitaev interactions in polar spin-orbit Mott insulators, *Phys. Rev. B* **101**, 100410 (2020).
- [72] See Supplemental Material for magnetic anisotropy in $\alpha\text{-RuCl}_3/\text{CrCl}_3$ and $\alpha\text{-RuCl}_3/\text{CrI}_3$.
- [73] H.-S. Kim, V. S. V., A. Catuneanu, and H.-Y. Kee, Kitaev magnetism in honeycomb RuCl_3 with intermediate spin-orbit coupling, *Phys. Rev. B* **91**, 241110 (2015).
- [74] C. Huang, J. Zhou, H. Wu, K. Deng, P. Jena, and E. Kan, Quantum anomalous Hall effect in ferromagnetic transition metal halides, *Phys. Rev. B* **95**, 045113 (2017).
- [75] Y. Tian, W. Gao, E. A. Henriksen, J. R. Chelikowsky, and L. Yang, Optically Driven Magnetic Phase Transition of Monolayer RuCl_3 , *Nano Lett.* **19**, 7673 (2019).
- [76] P. H. Souza, D. P. de Andrade Deus, W. H. Brito, and R. H. Miwa, Magnetic anisotropy energies and metal-insulator transitions in monolayers of $\alpha\text{-RuCl}_3$ and OsCl_3 on graphene, *Phys. Rev. B* **106**, 155118 (2022).
- [77] Y. Kubota, H. Tanaka, T. Ono, Y. Narumi, and K. Kindo, Successive magnetic phase transitions in $\alpha\text{-RuCl}_3$: XY-like frustrated magnet on the honeycomb lattice, *Phys. Rev. B* **91**, 094422 (2015).
- [78] K. A. Modic, R. D. McDonald, J. P. C. Ruff, M. D. Bachmann, Y. Lai, J. C. Palmstrom, D. Graf, M. K. Chan, F. F. Balakirev, J. B. Betts, G. S. Boebinger, M. Schmidt, M. J. Lawler, D. A. Sokolov, P. J. W. Moll, B. J. Ramshaw, and A. Shekhter, Scale-invariant magnetic anisotropy in RuCl_3 at high magnetic fields, *Nat. Phys.* **17**, 240 (2021).
- [79] B. Yang, Y. M. Goh, S. H. Sung, G. Ye, S. Biswas, D. A. S. Kaib, R. Dhakal, S. Yan, C. Li, S. Jiang, F. Chen, H. Lei, R. He, R. Valentí, S. M. Winter, R. Hovden, and A. W. Tsai, Magnetic anisotropy reversal driven by structural symmetry-breaking in monolayer $\alpha\text{-RuCl}_3$, *Nat. Mater.* **22**, 50 (2023).
- [80] S. Sinn, C. H. Kim, B. H. Kim, K. D. Lee, C. J. Won, J. S. Oh, M. Han, Y. J. Chang, N. Hur, H. Sato, B.-G. Park, C. Kim, H.-D. Kim, and T. W. Noh, Electronic structure of the Kitaev material $\alpha\text{-RuCl}_3$ probed by photoemission and inverse photoemission spectroscopies, *Sci. Rep.* **6**, 39544 (2016).
- [81] A. Koitzsch, C. Habenicht, E. Müller, M. Knupfer, B. Büchner, H. C. Kandpal, J. van den Brink, D. Nowak, A. Isaeva, and T. Doert, J_{eff} Description of the Honeycomb Mott Insulator $\alpha\text{-RuCl}_3$, *Phys. Rev. Lett.* **117**, 126403 (2016).
- [82] S. Biswas, Y. Li, S. M. Winter, J. Knolle, and R. Valentí, Electronic Properties of $\alpha\text{-RuCl}_3$ in Proximity to Graphene, *Phys. Rev. Lett.* **123**, 237201 (2019).
- [83] E. Gerber, Y. Yao, T. A. Arias, and E.-A. Kim, Ab Initio Mismatched Interface Theory of Graphene on $\alpha\text{-RuCl}_3$: Doping and Magnetism, *Phys. Rev. Lett.* **124**, 106804 (2020).
- [84] Y.-Z. You, I. Kimchi, and A. Vishwanath, Doping a spin-orbit Mott insulator: Topological superconductivity from the Kitaev-Heisenberg model and possible application to $(\text{Na}_2/\text{Li}_2)\text{IrO}_3$, *Phys. Rev. B* **86**, 085145 (2012).
- [85] S. Okamoto, Global phase diagram of a doped Kitaev-Heisenberg model, *Phys. Rev. B* **87**, 064508 (2013).
- [86] J. Schmidt, D. D. Scherer, and A. M. Black-Schaffer, Topological superconductivity in the extended Kitaev-Heisenberg model, *Phys. Rev. B* **97**, 014504 (2018).
- [87] U. F. P. Seifert, T. Meng, and M. Vojta, Fractionalized Fermi liquids and exotic superconductivity in the Kitaev-Kondo lattice, *Phys. Rev. B* **97**, 085118 (2018).
- [88] K. Nawa, Y. Imai, Y. Yamaji, H. Fujihara, W. Yamada, R. Takahashi, T. Hiraoka, M. Hagihala, S. Torii, T. Aoyama, T. Ohashi, Y. Shimizu, H. Gotou, M. Itoh, K. Ohgushi, and T. J. Sato, Strongly Electron-Correlated Semimetal RuI_3 with a Layered Honeycomb Structure, *J. Phys. Soc. Japan* **90**, 123703 (2021).
- [89] Y. Imai, K. Nawa, Y. Shimizu, W. Yamada, H. Fujihara, T. Aoyama, R. Takahashi, D. Okuyama, T. Ohashi, M. Hagihala, S. Torii, D. Morikawa, M. Terauchi, T. Kawamata, M. Kato, H. Gotou, M. Itoh, T. J. Sato, and K. Ohgushi, Zigzag magnetic order in the Kitaev spin-liquid candidate material RuBr_3 with a honeycomb lattice, *Phys. Rev. B* **105**, L041112 (2022).
- [90] D. A. Kaib, K. Riedl, A. Razpopov, Y. Li, S. Backes, I. I. Mazin, and R. Valentí, Electronic and magnetic properties of the RuX_3 ($X = \text{Cl}, \text{Br}, \text{I}$) family: two siblings—and a cousin?, *npj Quantum Mater.* **7**, 75 (2022).
- [91] D. Ni, X. Gui, K. M. Powderly, and R. J. Cava, Honeycomb-Structure RuI_3 , A New Quantum Material Related to $\alpha\text{-RuCl}_3$, *Adv. Mater.* **34**, 2106831 (2022).

S1. Magnetic anisotropy in $\alpha\text{-RuCl}_3/\text{CrCl}_3$ and $\alpha\text{-RuCl}_3/\text{CrI}_3$

We calculate the magnetic anisotropy energy for two heterostructures, $\alpha\text{-RuCl}_3/\text{CrCl}_3$ and $\alpha\text{-RuCl}_3/\text{CrI}_3$, by rotating the Cr moment from the most stable magnetic states obtained in the main text. The results for $\alpha\text{-RuCl}_3/\text{CrCl}_3$ are shown in Fig. S1 by rotations within (a) the ab plane and (b) the ac plane. In this case, the magnetic anisotropy in the CrCl_3 layer is less than 1 meV, indicating that the AFM interlayer interaction is in the order of 0.1 meV.

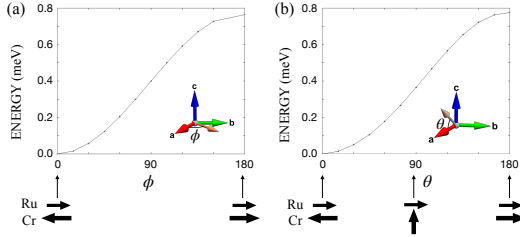


FIG. S1. Magnetic anisotropy energy in the CrCl_3 layer of $\alpha\text{-RuCl}_3/\text{CrCl}_3$ for the rotations of the Cr moment within (a) the ab plane and (b) the ac plane. The Ru moments are fixed along the $-a$ axis. The insets denote the definitions of the angles θ and ϕ . Schematics of the arrangements of Ru and Cr moments are shown below each panel.

Figure S2 shows the results for $\alpha\text{-RuCl}_3/\text{CrI}_3$. In this case, the magnetic anisotropy in the CrI_3 layer is about 3 meV, indicating that the interlayer interaction is also AFM but the strength is one order of magnitude larger than that in $\alpha\text{-RuCl}_3/\text{CrCl}_3$. Nonetheless, the most stable is not the interlayer AFM state but the state with the Cr moment canted by about 30 degrees from the c axis, presumably due to the strong out-of-plane anisotropy existing in the CrI_3 monolayer.

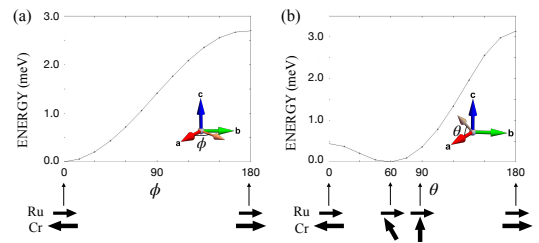


FIG. S2. Corresponding data for $\alpha\text{-RuCl}_3/\text{CrI}_3$. The notations are common to those in Fig. S1.